Excitation Mechanism of Mixed Rossby–Gravity Waves in the Equatorial Atmosphere: Role of the Nonlinear Interactions among Equatorial Waves

CARLOS F. M. RAUPP AND PEDRO L. SILVA DIAS

Department of Atmospheric Sciences, Institute of Astronomy, Geophysics, and Atmospheric Sciences, University of São Paulo, São Paulo, Brazil

(Manuscript received 9 July 2003, in final form 28 January 2004)

ABSTRACT

One possible explanation for the relatively high signal of the mixed Rossby–gravity waves observed in the tropical atmosphere is explored in this paper. This explanation is based on the nonlinear interactions among equatorial waves, and is made by adopting the nonlinear shallow water equations on the equatorial β plane. These equations are solved by a spectral method that uses the eigensolutions of the linear problem as the expansion basis. Numerical simulations are performed with a specified stationary mass source representative of the tropospheric heating associated with the typical convective activity over the Amazon Basin during the austral summer period. The numerical results show that the mixed Rossby–gravity waves are excited by a nonlinear mechanism in which the slow modes excited by the thermal forcing generate a quasigeostrophic basic state that supplies energy especially to the mixed Rossby–gravity waves with zonal wavenumbers 4 and 5, which have periods of the order of 4 days. The phase propagation of these unstable mixed modes leads to a periodic energy exchange between the mixed Rossby–gravity waves and the quasigeostrophic modes (Rossby and ultralong Kelvin modes). This regular nonlinear energy exchange implies a 4-day-cycle vacillation in the solution, which might be linked to the 4–6-day local oscillations in the dynamical field data throughout the Amazon region found in observational studies. Besides the importance of quasigeostrophic modes in the excitation of mixed Rossby–gravity waves, the numerical results also suggest that the predominance of the slow modes is crucial for maintaining the high signal of the unstable mixed modes, since these waves are strongly suppressed by the inclusion of the fast modes in the integration.

1. Introduction

The existence of wavelike motions with a period of the order of 4 and 5 days and wavelength of approximately 10 000 km (which corresponds to wavenumbers 4 and 5), with a structure very similar to the mixed Rossby–gravity waves (MRGW) predicted by Matsuno's theory of linear equatorial waves (Matsuno 1966), is a prominent characteristic of the tropical atmospheric circulation. Observational evidence of the signal of these kinds of motions in the equatorial region was initially obtained by Yanai and Maruyama (1966) and Maruyama (1967), who documented fluctuations in the meridional wind in the stratosphere with periods of 4–5 days associated with these particular waves. Other observational studies identified the signal of the MRGW in the troposphere, especially over the equatorial Pacific belt (Gruber 1974; Zangvil and Yanai 1980; Magaña and Yanai 1995; Dunkerton and Baldwin 1995; Pires et al. 1997; Wheeler and Kiladis 1999). Wheeler and Kiladis (1999), by performing a spectral analysis using outgoing longwave radiation (OLR) data, found that these waves are tightly coupled with convection and that the highest signal of the MRGW in the OLR series is located over the central Pacific near the date line.

Over the Atlantic sector, important observational evidence was obtained recently by Santos et al. (2002) by using a database of the National Centers for Environmental Prediction–National Center of Atmospheric Research (NCEP–NCAR) reanalysis from the period of the Amazon Boundary Layer Experiment, during April and May of 1987 (ABLE-2b). Figure 1, adapted from Santos et al. (2002), illustrates the power spectrum of the 850-hPa meridional wind component at the equator during the ABLE-2b period and over the Atlantic–Amazon longitudinal sector. Since the meridional wind at the equator is the best indicative quantity that characterizes the MRGW activity, Fig. 1 shows a high signal of MRGW perturbations with zonal wavelengths of 10 000–5000 km and periods of the order of 4–6 days over the Atlantic–South America equatorial sector. A very

Corresponding author address: Carlos F. M. Raupp, Rua do Matão, 1226—Cidade Universitária, São Paulo-SP, CEP, 05508-900, Brazil.
E-mail: cfmraupp@model.iag.usp.br

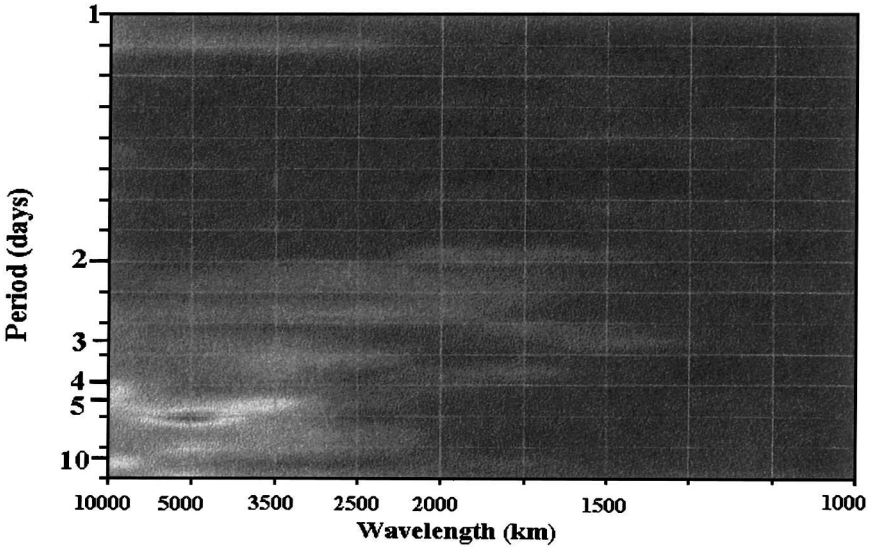

FIG. 1. Power spectrum of the meridional wind component at the equator, from the beginning up to 30th day of the ABLE-2b experiment. The abscissa axis represents wavelengths from 10 000 to 1000 km, while the ordinate axis corresponds to the period of the equatorial waves. The spectral analysis was evaluated over the longitudinal sector from Greenwich (near western African coast) up to 90°W (west of the Andes). (Adapted from Santos et al. 2002.)

similar spectrum of the meridional wind at the equator was obtained by Pires et al. (1997) for the Pacific sector using 4-month-period data of the Tropical Ocean Global Atmosphere Coupled Ocean–Atmosphere Response Experiment (TOGA COARE). Santos et al. (2002) showed that the antisymmetric-about-the-equator pattern of the horizontal divergence, associated with these MRGW perturbations, has an important role in the westward propagation of convective disturbances along the equatorial Atlantic region. When reaching the Amazon region, these convective anomalies exercise a strong control on the development of precipitation over this region. According to Santos et al., the westward propagation of squall lines, which develop along the north coast of South America, is triggered in the presence of an easterly regime over the Atlantic sector by perturbations associated with the MRGW originating in the equatorial Atlantic. An easterly regime is important in order to change the sign of the MRGW group velocity, which is eastward for a basic state at rest (Matsuno 1966). The implied equivalent depth found by Santos et al. for the MRGW observed in Fig. 1 is around 18 m over the Atlantic Ocean and around 7 m over the continent. This slowdown of the wave propagation velocity is related to the convection that is more intense over the Amazon region than the ocean during the austral summer period, as will be discussed in section 4.

As the stratospheric equatorial waves have the same spectral characteristics (wavenumber and frequencies) as the tropospheric ones and the MRGW have an upward energy transport, it is believed that stratospheric MRGW are directly forced by the correspondent convectively coupled tropospheric ones (Wheeler et al. 2000). In fact, as found initially by Holton (1972) and later noted by Salby and Garcia (1987) and Bergman and Salby (1994), oscillations in the diabatic heating associated with tropical convection can generate equatorial waves in the stratosphere such as Kelvin waves and MRGW. Holton found that a tropospheric heating of narrow longitudinal extent and antisymmetric about the equator with a standing oscillation of 4 to 5 days generates stratospheric MRGW with the same period.

Nevertheless, the tropospheric excitation mechanism that triggers these equatorially trapped waves is still debatable. Two important theories on the generation and scale selection of MRGW observed in the equatorial troposphere have been proposed. One is the lateral forcing theory proposed by Mak (1969). According to this theory, the MRGW are excited by wavelike disturbances that are generated in middle latitudes and propagate toward the tropical region. Mak (1969) examined the response of a two-layer model of the tropical atmosphere to stochastic forcing at lateral boundaries (30°N and 30°S). Mak found large responses in the model at wavenumbers and frequencies corresponding to the observed MRGW and a gravest Rossby mode. Similarly, Lamb (1973) studied the response of a model of the tropical atmosphere to midlatitude forcing, including the effects of condensational heating in the Tropics. Lamb suggested that the tropical atmosphere selectively responds to lateral forcing by generating equatorial wavelike disturbances with wavenumbers and frequencies similar to the observed MRGW and the gravest Rossby mode. In Lamb's theory, the waves are enhanced by the effect of condensational heating.

The other hypothesis is the so-called wave-conditional instability of the second kind (wave-CISK) theory initially proposed by Hayashi (1970). In this context, the interaction between equatorial waves' dynamics and cumulus convection can produce unstable modes whose structures resemble the MRGW. In fact, the range of vertical wavelengths of the unstable modes obtained by Hayashi's linear wave-CISK theory is rather similar to the vertical scales of the observed MRGW. Nonetheless, as observed by Hayashi (1970), the wave-CISK mechanism by itself cannot explain the selection of the zonal wavenumber and period. While the linear wave-CISK parameterization of the diabatic heating produces the most intense instability on the shortest Kelvin and gravity waves (linear wave-CISK catastrophe), in the nonlinear parameterization the most unstable mode is the Kelvin wave with zonal wavenumber 1 (Lau and Peng 1987; Hayashi and Sumi 1986), which has a period of 40 to 50 days and is associated with the Madden–Julian oscillation (Madden and Julian 1972, 1994).

However, even though these studies showed that the interaction between equatorial waves and cumulus convection by itself does not reproduce the selection of the observed scale of MRGW, Zangvil and Yanai (1981) found that the cloud cover in the Tropics has the same spectral peaks in wavenumber and frequency as the waves (see also Gruber 1974; Takayabu 1994; Wheeler and Kiladis 1999). This concordance suggests that there is a strong coupling between the waves and moist convection. A series of numerical experiments by the Geophysical Fluid Dynamics Laboratory (GFDL) general circulation model (Hayashi and Golder 1978) also shows that both midlatitude forcing and interaction with cumulus convection are important for the excitation of Yanai waves (see also Hayashi 1974). Hayashi and Golder concluded that Kelvin waves and MRGW can be generated by the effect of the latent heat release even if midlatitude disturbances are absent, but MRGW are significantly intensified when midlatitude disturbances propagate intermittently toward the equator. Itoh and Ghil (1988) argued that MRGW are produced by the nonlinear wave-CISK mechanism, while the lateral forcing selects the horizontal wavenumber. Recently, Magaña and Yanai (1995) obtained observational evidence that highlights the role of midlatitude disturbances for the excitation of MRGW in the equatorial troposphere. Using a 13-yr database of 200-hPa wind and OLR, Magaña and Yanai showed that the signal of Yanai waves in the tropical troposphere is enhanced in the presence of equatorial westerlies. The presence of equatorial westerlies favors the propagation of midlatitude disturbances toward the equator (Webster and Holton 1982; Arkin and Webster 1985; Tomas and Webster 1994; and others).

In this paper, we perform numerical simulations with a rather simplified model of the tropical atmospheric motions (shallow water model on the equatorial β plane). Despite not considering either lateral forcing or parameterization of the feedback between equatorial waves and moist convection, we found in some of our numerical results a highly prominent signal of MRGW with a spatial structure of zonal wavenumbers 4 and 5 and a period of the order of 4 days. Thus, this paper explores a possible explanation for the relatively high magnitude of MRGW observed in the tropical atmosphere in terms of the dynamics of the simple model used. This explanation is based on the nonlinear interactions among equatorial waves. The nonlinear shallow water model is solved in the spectral form using the normal modes of the linearized version about a basic state at rest (that is, the Matsuno waves). Numerical simulations are performed with a stationary mass source representative of the heating produced by the typical convective activity on the Amazon region during the austral summer period. It is suggested that both excitation and scale selection of the MRGW observed in the tropical atmosphere can be generated by instability of the basic state associated with the quasigeostrophic modes (Rossby and ultralong Kelvin modes) resonantly excited by the stationary part of tropical convective heat sources. The numerical results also show that the nonlinear interactions between MRGW and Rossby waves (RW) imply a vacillation in the numerical solution with a cycle determined by the period of the MRGW (approximately 4 days). This vacillation is probably associated with local oscillations in the vorticity and wind fields throughout the Amazon region detected in the observational work of Santos et al. (2002).

The numerical results presented in this work are interpreted in terms of the theoretical framework of nonlinear interactions among equatorial waves developed by Ripa (1982, 1983a,b). Ripa (1982, 1983a), using the same model and formalism as the present work, developed a theory concerning the nonlinear interactions among equatorial waves based on the phase space expansion of some integrals of motion of the system. In this context, Ripa obtained some constraints that the coupling coefficients must satisfy in order to ensure the invariance of such quadratic (to lowest order) integrals of motion. A straightforward view of Ripa's formalism will be carried out here in order to organize the theoretical framework.

In section 2, the basic governing equations and the spectral method of solution are described. The theoretical framework employed by Ripa (1983a) on nonlinear interactions among equatorial waves is carried out in section 3. Section 4 presents numerical results for a specified stationary mass source with spatial scales that roughly simulate the heating produced by the typical convective activity on the Amazon Basin during the Southern Hemisphere summer. We show numerical solutions that contain only the MRGW inserted in the Rossby category and the quasigeostrophic modes, as well as numerical results with the complete spectrum,

that is, with the addition of the inertio-gravity and divergent (zonally asymmetric) Kelvin waves. Results in the absence of purely geostrophic modes (wavenumber 0) and zonally asymmetric Rossby waves in the solution are also explored in order to test the sensitivity of the excitation of MRGW to the presence of these modes. A comparison between linear and nonlinear solutions is also presented in that section. The summary of the main insights of this work and implications are discussed in section 5, as well as some suggestions for future investigations.

2. Model equations and solution method

The shallow water model on the equatorial β plane adopted in the present work can be described by the following system of equations in the vector form:

$$\frac{\partial \boldsymbol{\xi}}{\partial t} + \boldsymbol{\Omega}\boldsymbol{\xi} = \mathbf{F} + \mathbf{N} - \kappa\boldsymbol{\xi} - \nu\nabla^4\boldsymbol{\xi}. \tag{2.1}$$

System (2.1) is shown after normalization, using the scales $L = (c/\beta)^{1/2}$ and $T = (1/c\beta)^{1/2}$ of length and time, respectively, and H as the vertical scale, where $\boldsymbol{\xi} = [u(x, y, t), \upsilon(x, y, t), \phi(x, y, t)]^{\mathrm{T}}$, $\mathbf{F} = [0,0,F_\phi]^{\mathrm{T}}$, and the terms

$$\boldsymbol{\Omega} = \begin{bmatrix} 0 & -y & \dfrac{\partial}{\partial x} \\ y & 0 & \dfrac{\partial}{\partial y} \\ \dfrac{\partial}{\partial x} & \dfrac{\partial}{\partial y} & 0 \end{bmatrix} \quad \text{and}$$

$$\mathbf{N} = \begin{bmatrix} -\left(u\dfrac{\partial u}{\partial x} + \upsilon\dfrac{\partial u}{\partial y}\right) \\ -\left(u\dfrac{\partial \upsilon}{\partial x} + \upsilon\dfrac{\partial \upsilon}{\partial y}\right) \\ -\left(u\dfrac{\partial \phi}{\partial x} + \upsilon\dfrac{\partial \phi}{\partial y}\right) - \phi\left(\dfrac{\partial u}{\partial x} + \dfrac{\partial \upsilon}{\partial y}\right) \end{bmatrix}$$

are the linear operator associated with the linearized equations and the nonlinear term, respectively. Here, u and υ are the components of the two-dimensional velocity field on the x (eastward) and y (northward) directions, respectively; ϕ is the geopotential field, $c = \sqrt{gH}$ is the phase speed of pure gravity waves, H is the equivalent depth, and g is the effective gravity acceleration. The term F_ϕ represents the mass source and can also be interpreted as a heat source. The term $-\kappa\boldsymbol{\xi}$ represents the simplest form to parameterize restoring forces that arise whenever the system is perturbed from rest. In this case, κ corresponds to the Rayleigh drag coefficient in the momentum equations and the rate coefficient for Newtonian cooling in the continuity equation. This linear damping term is necessary for the solution in order to attain a permanent regime in the presence of the heat source. The parameter $\beta = df/dy$ is the Rossby parameter (where f is the Coriolis parameter) and is assumed here as a constant and with its equatorial value. The term $-\nu\nabla^4\boldsymbol{\xi}$ is the biharmonic diffusion term and its presence in (2.1) is necessary in order to avoid an unrealistic accumulation of energy on the shortest waves retained on the truncation of the spectrum due to the effects of direct energy cascade.

Apart from representing the evolution of a single layer of homogenous and hydrostatic fluid, system (2.1) can also be regarded as the governing equations for the horizontal structure associated with a particular vertical mode of the vertical structure equation of an upper-lidded atmospheric model. In this context, the equivalent depth H is the separation constant and is obtained as an eigenvalue of the vertical structure equation. The mass source F_ϕ in this case can be thought of as the projection of the vertical derivative of the diabatic heating on the right-hand side of the thermodynamic equation onto the particular vertical mode (Silva Dias et al. 1983). Lindzen et al. (1968) argued that considering a rigid upper boundary condition in the primitive equations can introduce spurious free oscillations that do not appear in vertical unbounded atmospheric models. These free oscillations appear as spurious resonances when analyzing forced oscillations. However, despite the limitations of vertically bounded atmospheric models, models based on vertical normal mode decomposition have shown to be very useful in explaining dynamical features of observed atmospheric phenomena. This is demonstrated in numerous studies (see, e.g., Kasahara and Silva Dias 1986; Lim and Chang 1986; Kasahara 1984; Kasahara and Tanaka 1989; Wang and Xie 1996; DeMaria 1985; Silva Dias et al. 1983, 1987; Fulton and Schubert 1985; Gill 1980; Silva Dias and Bonatti 1985; and many others).

Zonal periodicity and bounded solution as $|y|$ goes to infinity provide the necessary conditions to compute the eigensolutions of $\boldsymbol{\Omega}$, which are used as a basis in the expansion of $\boldsymbol{\xi}$ and all other terms in (2.1) as in

$$\mathbf{G}(x, y, t) = \sum_{k=-\infty}^{+\infty} \sum_{n=-1}^{\infty} \sum_{r=1}^{3} \mathbf{g}_{k,n,r}(t)\boldsymbol{\xi}_{k,n,r}(y)e^{ikx}, \tag{2.2}$$

where $\mathbf{G}(x, y, t) = [g_1(x, y, t), g_2(x, y, t), g_3(x, y, t)]^{\mathrm{T}}$ is a generic vector function, k is the zonal wavenumber, n is the meridional mode, which distinguishes the meridional structure of the eigenfunctions $\boldsymbol{\xi}_{k,n,r}(y)$ of $\boldsymbol{\Omega}$; $r = 1$ for RW, $r = 2$ for inertio-gravity waves propagating westward (WGW), and $r = 3$ for inertio-gravity waves propagating eastward (EGW). The MRGW correspond to the $n = 0$ mode and are included in the $r = 1$ (for $k > 2^{-1/2}$) and $r = 2$ (for $k < 2^{-1/2}$) category. The Kelvin wave is represented by $n = -1$ and $r = 3$. The determination of the eigenfunctions of $\boldsymbol{\Omega}$ and a complete discussion on the properties of such free linear wave solutions of the governing equations are found in Matsuno (1966).

In the presence of the nonlinear term $\mathbf{N}(x, y, t)$, system (2.1) is no longer separable and, strictly speaking, the linear equatorial waves no longer exist as normal modes. However, if the amplitude of the state variables is relatively small (but finite), the representation of the solution obtained by expansion (2.2) is still valid. This is exactly the case for the numerical simulations shown in section 4. In this case, the superposition of linear waves constitutes the dominant part of the solution and the nonlinear term can be regarded as an interaction mechanism through which the linear wave modes can exchange energy, as will be shown in section 3. Thus, except in some fully turbulent motions such as the boundary layer atmospheric flow and hydraulic jumps, or the case of intense hydrodynamic instability associated with highly sheared flows, the concept of linear free-wave modes remains useful for the physical understanding of the mathematical solutions and for interpreting observed atmospheric motion. This is demonstrated by the success of the normal mode initialization techniques used in numerical weather prediction. Moreover, as discussed in section 1, there are several observational evidences reinforcing the idea that the linear waves are effectively observed in nature. In this study, we shall use the concept of linear eigenmodes in a similar way and regard the nonlinear term **N** as effects through which the equatorial waves exchange energy.

Therefore, substitution of (2.2) in (2.1), multiplication by the conjugate of the eigenfunctions $\boldsymbol{\xi}_{k,n,r}(y)$ and global integration lead to

$$\frac{dc_{k,n,r}(t)}{dt} - i\omega_{k,n,r}c_{k,n,r}(t) = f_{k,n,r}(t) + \eta_{k,n,r}(t) - (\kappa + k^4\nu)c_{k,n,r}(t) - \nu d_{k,n,r}(t), \tag{2.3}$$

where $c_{k,n,r}(t)$, $f_{k,n,r}(t)$, $\eta_{k,n,r}(t)$, and $d_{k,n,r}(t)$ are the spectral coefficients of the state vector $\boldsymbol{\xi}(x, y, t)$, the forcing vector $\mathbf{F}(x, y, t)$, the nonlinear term $\mathbf{N}(x, y, t)$, and the meridional component $\partial^4\boldsymbol{\xi}/\partial y^4$ of the biharmonic diffusion, respectively. The parameters $\omega_{k,n,r}$ represent the eigenfrequencies associated with the free linear wave solutions of the model. The numerical integration scheme of (2.3) assumes that the coefficients $f_{k,n,r}(t)$, $\eta_{k,n,r}(t)$, and $d_{k,n,r}(t)$ are constant during a very short time $2\Delta t$ so that, given the coefficients $c_{k,n,r}(t - \Delta t)$, $d_{k,n,r}(t - \Delta t)$, and $\eta_{k,n,r}(t)$, an analytic solution can easily be obtained at $t + \Delta t$. The convolution coefficient $\eta_{k,n,r}(t)$ is evaluated here in the pseudospectral form by calculating the nonlinear term **N** in the physical space and then projecting it onto the phase space. The principal advantage of the semianalytic method employed here is the correct representation of the energy dispersion by the fast linear waves, which is important to the geostrophic adjustment process (Silva Dias et al. 1983).

3. Ripa's theory on nonlinear energy exchanges among equatorial waves

In the previous section we showed the solution of the governing equation (2.1) in the spectral form. In this method, the nonlinear term is evaluated in a pseudospectral representation. Although this technique substantially reduces the amount of calculations, it does not permit a fine analysis of nonlinear wave–wave interactions since it is entirely numerical. On the other hand, many authors have used spectral models with few terms in the expansion in order to gain physical understanding of interaction mechanisms. In such highly truncated models, the nonlinear terms are developed and interaction coefficients can be explicitly calculated. The values and mathematical properties of these coefficients give precise information about nonlinear evolution of the system and stability of the waves. Therefore, even though we did not adopt the interaction coefficient method in the integration of (2.3), this methodology is used in this section in order to theoretically explore interacting properties associated with the invariance of two particular integrals of motion. The theoretical framework developed in this section follows the formalism of Ripa (1983a) and is important in order to physically interpret the numerical results shown in section 4.

System (2.1) is constrained by the existence of several integrals of motion. Two (and only two) of them have, to lowest order, a quadratic dependence in terms of the dependent variables of the model. The consequences of their conservation to the evolution of (2.1) in the phase space are more powerful than the consequences of the other conservation laws. These quadratic-to-lowest- order integrals of motion are the total energy E and the total pseudomomentum P defined by their respective densities

$$E = \frac{1}{2}[(u^2 + \upsilon^2 + \phi^2) + \phi(u^2 + \upsilon^2)] \tag{3.1a}$$

and

$$P = \phi u - \frac{1 + \phi}{2}(q - y)^2, \tag{3.1b}$$

where q is the potential vorticity and y refers to the nondimensional Coriolis parameter. Following Ripa (1983a), we decompose the energy and pseudomomentum and express their invariance as

$$E^{(2)} + E^{(3)} = \text{const} \tag{3.2a}$$

and

$$P^{(2)} + P^{(3)} + O(u, \upsilon, \phi)^4 = \text{const}, \tag{3.2b}$$

where

$$E^{(2)} = \int_{-L_x}^{L_x}\int_{-\infty}^{+\infty}\frac{1}{2}(u^2 + \upsilon^2 + \phi^2)dxdy,$$

$$E^{(3)} = \int_{-L_x}^{L_x}\int_{-\infty}^{+\infty}\frac{1}{2}\phi(u^2 + \upsilon^2)dxdy, \tag{3.2c}$$

$$P^{(2)} = \int_{-L_x}^{L_x}\int_{-\infty}^{+\infty}\left(u\phi - \frac{1}{2}\Psi^2\right)dxdy,$$

$$P^{(3)} = -\frac{1}{2}\int_{-L_x}^{L_x}\int_{-\infty}^{+\infty}\phi\Psi^2 dxdy, \qquad (3.2d)$$

where $\Psi = \partial v/\partial x - \partial u/\partial y - f\phi$ is the first-order deviation of the potential vorticity from its equilibrium value ($q_0 = f$). From Parseval's theorem, the expansion basis used here provides a diagonal representation of the quadratic part of total energy and pseudomomentum:

$$E^{(2)} = \frac{1}{2}\sum_a c_a c_a^* = \frac{1}{2}\sum_a |c_a|^2;\ \mathrm{P}^{(2)} = \frac{1}{2}\sum_a s_a|c_a|^2. \qquad (3.3)$$

The subscript a in (3.3) indicates a particular expansion mode characterized by (k, n, r), that is, $a = (k, n, r)$ and * refers to the complex conjugate. The parameter s in the phase space expansion of the quadratic part of pseudomomentum in (3.3) is the zonal slowness index (Hayes 1974; Ripa 1981, 1982, 1983a,b), which is defined as the inverse of the zonal phase speed. The classification of the equatorial waves in terms of the zonal slowness **s** is given in Table 1. It is interesting that the RW, WGW, EGW, MRGW, and Kelvin waves (KW) are clearly separated on the slowness space. The double behavior of the MRGW is also clearly explicit on the slowness space. The MRGW are inserted in the Rossby category for $s < -1$ and in the gravity category for $-1 < s < 0$. To clarify the classification of the equatorial waves on the s space, Table 2 shows the asymptotic values of s corresponding to short and long waves, as well as the approximated relation $\omega(k)$ and the possible kinds of equatorial waves on each of such limits.

The phase space expansion of the cubic part of total energy and pseudomomentum are obtained by replacing u, v, and ϕ in (3.2) for their corresponding expansion in terms of the basis functions used in this work. The end result is

$$E^{(3)} = \frac{1}{2}\mathrm{Re}\left[\sum_a\sum_b\sum_c(-i)c_a c_b c_c S_{abc}\right],$$

$$P^{(3)} = \frac{1}{2}\mathrm{Re}\left[\sum_a\sum_b\sum_c c_a c_b c_c(-i)U_{abc}\right], \qquad (3.4a)$$

where

TABLE 1. Equatorial wave types of RW ($n \geq 1$), GW ($n > 0$), MRGW ($n = 0$), and KW ($n = -1$) as function of the slowness. (Adapted from Ripa 1983a.)

RW	MRGW	GW	KW
$n \geq 1$	$n = 0$	$n > 0$	$n = -1$
$-\infty < s \leq -2n-1$	$-\infty < s < 0$	$-1 < s < 1$	$s = 1$

TABLE 2. Asymptotic values of s and their corresponding characteristic zonal wavenumber, frequencies, and types of oscillations. (Adapted from Ripa 1983a.)

$s \approx$	$-\infty$	$-2n-1$	-1	0	1
$k \approx$	∞	0	∞	0	∞
$\omega \approx$	$-1/k$	$-k/(2n+1)$	k	$\pm(2n+1)^{1/2}$	$-k$
$n \geq$	0	1	1	0	-1
Wave type	RW or MRGW	RW	GW	GW or MRGW	GW or KW

$$S_{abc} = i\delta_{abc}\int_{-\infty}^{+\infty}\{\phi_a(y)[u_b(y)u_c(y) + v_b(y)v_c(y)] + \mathrm{CP}\}dy, \qquad (3.4b)$$

$$U_{abc} = -i\delta_{abc}\int_{-\infty}^{+\infty}(\phi_a\Psi_b\Psi_c + \mathrm{CP})dy. \qquad (3.4c)$$

Here, CP means cyclical permutations of (a, b, c) modes. In (3.4c), $\Psi_a(\equiv ik_a v_a - du_a/dy - f\phi_a)$ is the deviation of potential vorticity, defined earlier, associated with the eigenfunction $\boldsymbol{\xi}_a(y)$. The coefficient δ_{abc} represents the interaction condition for the triad (a, b, c) and is given by $\delta_{abc} = 2(c/\beta)^{1/2}\delta(k_a + k_b + k_c)$ if the sum of the three meridional modes is odd or $\delta_{abc} = 0$ if the sum is even (see Busbridge 1948; Domaracki and Loesch 1977), where Kronecker's delta function δ results from the orthogonality of the trigonometric functions used in the expansion on the x direction.

On the other hand, substituting the state variables of the model and their spatial derivatives in the nonlinear term **N** by their respective spectral expansion, the evolution equation on the phase space (2.3), in the absence of forcing and damping terms, can be written in terms of the interaction coefficients as

$$\frac{dc_a(t)}{dt} - i\omega_a c_a(t) = -\sum_b\sum_c \sigma_a^{bc} c_b(t)c_c(t), \qquad (3.5)$$

where σ_a^{bc} is the coupling (interaction) coefficient among the modes a, b, and c, given by

$$\sigma_a^{bc} = \left\langle\left\{u_b(y)ik_c\boldsymbol{\xi}_c(y) + v_b(y)\frac{d\boldsymbol{\xi}_c(y)}{dy} + [0,0,1]^{\mathrm{T}}\phi_b(y)\left[ik_c u_c(y) + \frac{dv_c(y)}{dy}\right] + \mathrm{CP}\right\}\cdot\boldsymbol{\xi}_a^*(y)\right\rangle\delta_{abc}. \qquad (3.6)$$

Like the coefficients S_{abc} and U_{abc}, the coupling coefficients σ_a^{bc} are real. Any of these coefficients are also invariant under permutation of either the subscripts or the superscripts. Physically, the coupling coefficient σ_a^{bc} represents the projection onto the mode a of the advection of the wind and mass fields associated with mode c by the velocity field produced by mode b, and the product between the mass field produced by mode

b and the horizontal divergence produced by mode c, and vice versa ($b \leftrightarrow c$). From (3.5) it follows that

$$\frac{d|c_a(t)|^2}{dt} = \sum_b \sum_c \sigma_a^{bc} \,\mathrm{Re}(c_a c_b c_c),$$
$$\frac{dc_a c_b c_c}{dt} = i(\omega_a + \omega_b + \omega_c) c_a c_b c_c + O(c^4). \quad (3.7)$$

Replacing the above equation in (3.3) and (3.4) and using the result in the time derivative of (3.2a)–(3.2b) we get

$$\sum_a \sum_b \sum_c [\sigma_a^{bc} + S_{abc}(\omega_a + \omega_b + \omega_c)] \,\mathrm{Re}(c_a c_b c_c) + O(c^4) = 0, \quad (3.8a)$$

$$\sum_a \sum_b \sum_c [s_a \sigma_a^{bc} + U_{abc}(\omega_a + \omega_b + \omega_c)] \,\mathrm{Re}(c_a c_b c_c) + O(c^4) = 0. \quad (3.8b)$$

Since these equations must hold for any state of the system, $c_a c_b c_c$ is completely arbitrary (besides its invariance under permutations). Therefore, the symmetric part of the expression between square brackets in (3.8) must vanish for all interacting triads, namely,

$$\sigma_a^{bc} + \sigma_b^{ac} + \sigma_c^{ab} = -3S_{abc}(\omega_a + \omega_b + \omega_c), \quad (3.9a)$$

$$s_a \sigma_a^{bc} + s_b \sigma_b^{ac} + s_c \sigma_c^{ab} = -3U_{abc}(\omega_a + \omega_b + \omega_c). \quad (3.9b)$$

The constraints (3.9a)–(3.9b) have some interesting implications for the dynamics of the equatorial waves studied in the present work. Especially, if the triad (a, b, c) satisfies the resonance condition ($\omega_a + \omega_b + \omega_c = 0$), the coupling coefficients satisfy the relation $\sigma_a^{bc} : \sigma_b^{ac} : \sigma_c^{ab} :: s_b - s_c : s_a - s_c : s_a - s_b$. Thus, in such resonant interactions, the component of the triad that has the coupling coefficient with the opposite sign of the other two (and, consequently, with the greatest absolute value) has the intermediate slowness. Thus, in this kind of interaction, the wave with the intermediate slowness gains energy from (or releases energy to) the other two, more explicitly,

$$\Delta E_a + \Delta E_b + \Delta E_c = 0, \quad (3.10a)$$

$$s_a \Delta E_a + s_b \Delta E_b + s_c \Delta E_c = 0. \quad (3.10b)$$

Here, Δ denotes the change of energy due to interaction with the other two components. This condition of cascade/decascade shown above is a generalization of Fjörtoft's theorem (Fjörtoft 1953), but on the slowness space, instead of on the total wavenumber space as is the case in the barotropic nondivergent model. Furthermore, using the definition of the slowness s (inverse of the phase speed of the wave) and the interaction condition ($k_a + k_b + k_c = 0$), it is easy to show that the wave with the intermediate slowness in a certain resonant triad has the greatest absolute frequency of the triad. Thus, in a resonant triad, the wave with the largest absolute frequency gains energy from (or releases energy to) the other two. The immediate consequence of this constraint is that the absolutely geostrophic modes (zonally symmetric Rossby and Kelvin modes) are always stable in a resonant interaction. These geostrophic modes can only be unstable and supply energy to the other equatorial waves by off-resonant interactions and this restriction inhibits instabilities of these modes, as we will see in the numerical results shown in section 4. The conditions (3.9) and (3.10) also imply that resonant interactions conserve the quadratic (lowest order) part of total energy and pseudomomentum; the changes of $O(c^3)$ terms are caused by interactions by off-resonant triads.

In the case of the quasigeostrophic shallow water model at midlatitude β plane studied by Ripa (1981), the total energy and pseudomomentum are exactly quadratic integrals. Thus, in such a system, the generalization of Fjörtoft's theorem given by the condition (3.10) is valid for all triads (not only for resonant ones), and the total energy and pseudomomentum are conserved for an arbitrary truncation of the expansion basis to all orders in amplitudes.

In the shallow water model on the equatorial β plane adopted in the present work, the quasigeostrophic approximation cannot be made ($f_0 = 0$). However, the present model allows the presence of Rossby waves and these waves are quasigeostrophic. Thus, in the present model, the properties valid for interacting triads of the quasigeostrophic model of midlatitudes are essentially valid for interacting triads involving only Rossby waves. Therefore, for the model used here, the conservation of the quadratic part of total energy and pseudomomentum, and consequently the condition of cascade/decascade in the slowness space given by (3.10), is exactly valid for the resonant triads and essentially valid for triads that contain only quasigeostrophic waves. Moreover, for the quasigeostrophic waves the pseudomomentum and slowness are essentially the potential enstrophy and the total wavenumber squared, respectively. As a consequence, the cascade/decascade condition on the slowness space directly reflects a similar condition on the zonal wavenumber and meridional mode spaces. In this sense, a direct energy cascade toward high zonal wavenumbers and meridional modes is not permitted in this kind of interaction.

The properties of energy exchanges among equatorial waves discussed above are consequences of the constraints (3.9a)–(3.9b). These constraints, on the other hand, are consequences of the conservation of E and P, which is rigorously valid only in the absence of forcing and damping terms. However, in the presence of a stationary forcing and a damping term, the solution, after a transient period, attains a permanent regime during which the total energy is conserved. Therefore, the constraints (3.9a)–(3.9b) are absolutely valid for the numerical simulations shown in the following section after the solutions reach the permanent regime due to the balance between the forcing and damping terms. Fur-

thermore, during the transient period, those constraints may also be as valid as the numerical solutions approximate to such a permanent regime, as we shall see later.

4. Results of numerical simulations

In this section we show results of numerical integration of the initial value problem (2.1) for a specified stationary mass source given by

$$F_\phi = F_0 \exp\left[-\left(\frac{x - x_0}{r_e}\right)^2 - \left(\frac{y - y_0}{r_e}\right)^2 \right], \quad (4.1)$$

with y_0 and x_0 corresponding to approximately 11°S and 65°W, respectively, and $r_e = 800$ km as in Silva Dias et al. (1983) to simulate the effect of heat sources in the Amazon and central Brazil. The analysis performed in this section assumes that the equivalent depth of the shallow water equation model (2.1) is of the order of 250 m. This value is associated with the equatorial response to typical tropical heat sources, which project the most part of energy onto the internal mode corresponding to that value of H (DeMaria 1985; Silva Dias and Bonatti 1985). This particular internal mode is characterized by only one phase inversion in the troposphere (occurring in the midtroposphere) and highest signals occurring at around 850 and 200 hPa (Fulton and Schubert 1985; DeMaria 1985; Kasahara and Silva Dias 1986). On the other hand, observational studies have shown that equatorial waves in the troposphere tend to show an implied equivalent depth around 25 m (Wheeler and Kiladis 1999; Wheeler et al. 2000; Takayabu 1994). However, this implied equivalent depth of equatorial waves found in observational studies is believed to be a result of the interaction between moist convection and large-scale dynamics. In fact, if one assumes that the convective forcing is proportional to divergence, in a first approximation, the divergent term in the continuity equation of system (2.1) appears multiplied by an effective equivalent depth that is smaller than the true equivalent depth H. The stronger the convection related to the divergence, the smaller the effective equivalent depth. Thus, the equivalent height (H), and consequently, the characteristic wave speed (c), will be smaller than those of the free waves and the magnitude reduction is proportional to the intensity of the convective term in the right-hand side of the continuity equation. Since the main concern in this paper is to analyze only the role of weakly nonlinear interactions among equatorial waves as another possible excitation mechanism of MRGW, other physical mechanisms such as the feedback between equatorial wave dynamics and moist convection were not included in our model in order to isolate the physical mechanism with which we are concerned. Therefore, we considered here the equivalent depth $H = 250$ m representative of equatorial waves forced by convection but uncoupled with convection. The role of reducing the equivalent depth of the model, which implies the incorporation of the interaction between convection and dynamics in the model (2.1), on the excitation of MRGW by the nonlinear mechanism explored in this work would be an interesting subject for a future work.

The numerical simulations presented in this section also assume a linear damping term of 10 days ($\kappa = 0.1$ day^{-1}) and the coefficient ν was chosen in order to produce a damping time of the order of 2 h for the smallest-scale waves retained in the model. The parameter F_0 in (4.1) is assumed to be equivalent to a heating ratio of 25 K day^{-1} or a precipitation ratio of 80 mm day^{-1}. These values are characteristic of typical convective episodes throughout the Amazon region (see, e.g., Halverson et al. 2002; Anagnostou and Morales 2002; Laurent et al. 2002). The initial condition in the numerical simulations shown in this section is one of no motion and no geopotential perturbation. Figure 2 shows the spatial distribution of wind and mass fields associated with the nonlinear numerical solution where only quasigeostrophic modes and MRGW inserted in the Rossby category ($k > 2^{-1/2}$) are considered in the integration. Figure 2a shows the solution at $t = 2.5$ days, while Fig. 2b shows the solution at $t = 20$ days. The interpretation of the model results in terms of the internal mode with $H = 250$ m implies that dynamical fields (shown in Figs. 2, 3, 5, and 9) can be regarded as being representative of the upper troposphere or lower troposphere with the reversed sign.

The slow dispersion of energy of Rossby waves away from the heat source, which results in the development of an anticyclonic circulation (known as the Bolivian high), can be clearly observed in Fig. 2. It is interesting to notice that even when most part of the energy is concentrated near the source region ($\approx$ 2.5 days), a noticeable flow perturbation extending through the whole zonal domain has already developed. Since it is impossible that the energy directly generated by the thermal forcing has been dispersed throughout the whole domain during such a short period by the equatorial waves, it is evident that this large zonal-scale perturbation is a result of internal mechanisms of energy conversion. At $t = 20$ days (Fig. 2b) we can observe an intensification of the meridional component of the wind field associated with this perturbation, implying an intensification of an anticyclonic circulation over the Caribbean–Central American region. Figure 3 shows that this large zonal-scale perturbation has a spatial structure very close to the MRGW, with an antisymmetric about the equator pattern in the divergence field that is exactly in phase with the maxima of the meridional wind along the equator. Figure 3 also shows that, even in the first few hours of integration, when the energy resulting directly from the forcing is very close to the region of the source, the magnitude of the horizontal divergence and meridional wind in a region so far from the heating are quite high. It is also clear from Fig. 3

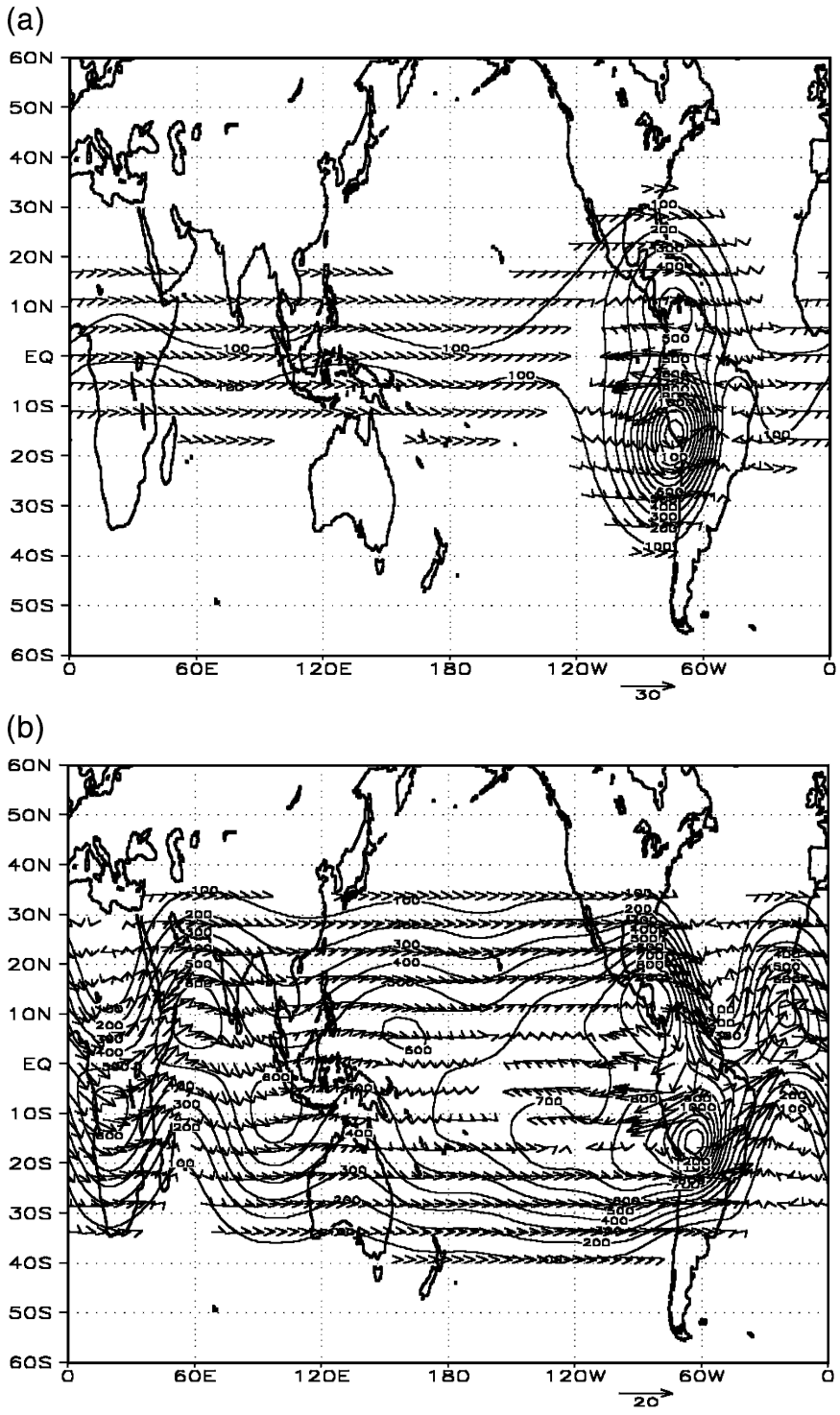

FIG. 2. Spatial structure of geopotential (contour) and wind (vector) fields corresponding to the nonlinear numerical solution in which only quasigeostrophic modes and MRGW inserted in the Rossby category ($k > 2^{-1/2}$) are considered in the integration. The solution at (a) t = 2.5 and (b) t = 20 days. The wind and geopotential fields are shown in m s^{-1} and m^2 s^{-2} respectively.

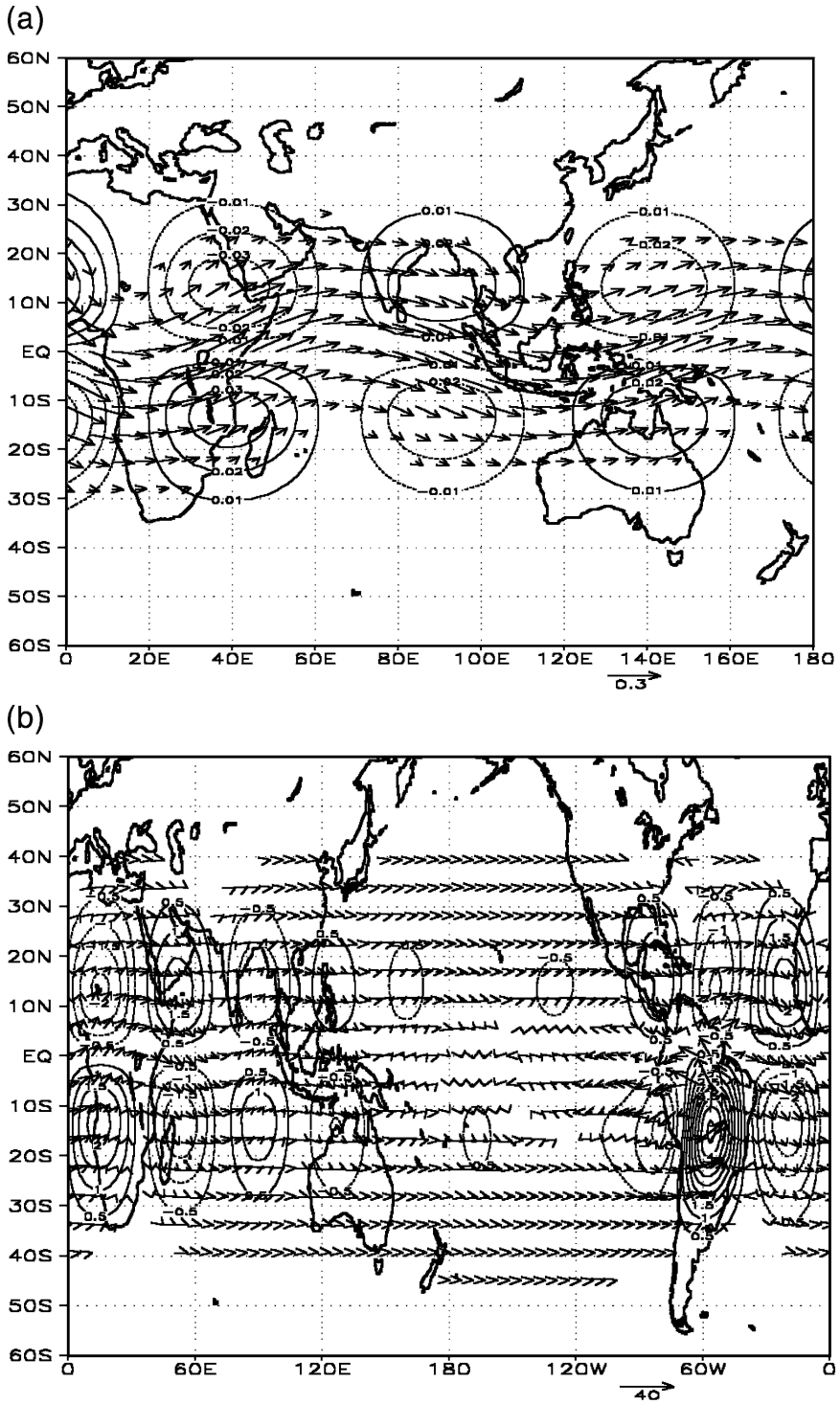

FIG. 3. Spatial structure of the horizontal divergence (contour) and wind (vector) fields associated with the same numerical solution as Fig. 2 at (a) $t = 6$ h and (b) $t = 30$ days. The wind and divergence fields are shown in m s^{-1} and 10^{-6} s^{-1} respectively.

that this perturbation resulting from any internal instability mechanism shows a well-defined zonal structure of zonal wavenumber 4 at the beginning of the integration (Fig. 3a) and zonal wavenumber 5 at $t = 30$ days (Fig. 3b), when the solution has already reached a permanent regime because of the balance between the forcing and linear damping terms (see Fig. 6). This excitation of MRGW with zonal wavenumbers 4 and 5 is

verified by Fig. 4, which shows the time evolution of the quadratic part of energy projected onto the MRGW with zonal wavenumbers 4 (closed circles) and 5 (open circles).

Figure 4 indicates that the quadratic energy associated with the MRGW increases as a function of time during the first 30 days of the integration, oscillating thereafter in the permanent regime attained by the numerical solution. The $k = 4$ and 5 (about 10 000 km) of the MRGW have similar magnitude at the beginning of the integration, but $k = 5$ dominates as time increases, as already shown in Fig. 3. Another feature that deserves attention is the oscillation of the MRGW energy observed in Fig. 4. During the whole period of integration, the quadratic part of total energy projected onto MRGW presents a well-defined cycle of approximately 4 days. This cycle is quite close to the 3.75–4.1-day theoretical period of the MRGW with zonal wavenumbers 4 to 5 and equivalent depth of 250 m. The MRGW activity is also noticeable in Fig. 5, which shows the meridional wind at the equator referring to the same numerical solution as Figs. 2–4. As discussed in section 1, the meridional wind at the equator is the best indicative quantity that characterizes the MRGW activity. It is

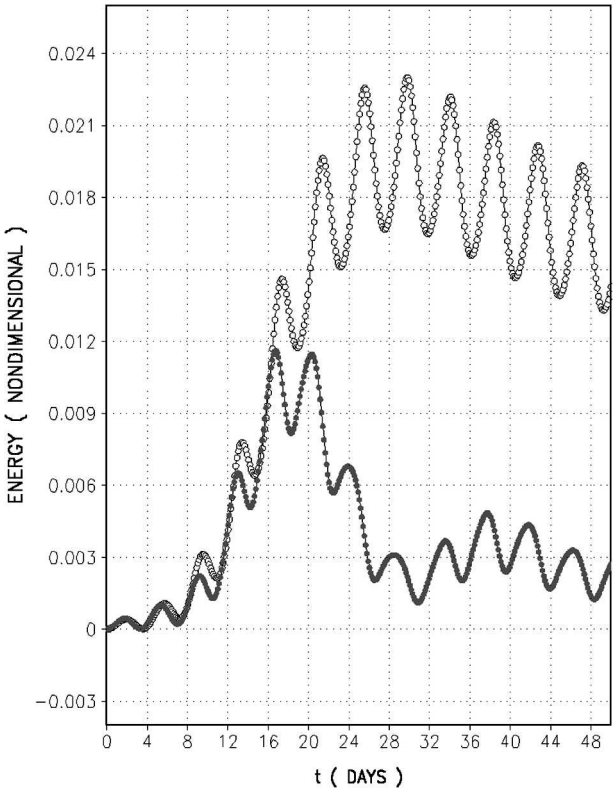

FIG. 4. Quadratic component of total energy associated with MRGW with $k = 4$ (closed circles) and $k = 5$ (open circles) associated with the same numerical solution as Figs. 2 and 3. The energy shown above is nondimensional, using the scales $[L]$ and $[T]$ defined in section 2 with $H = 250$ m.

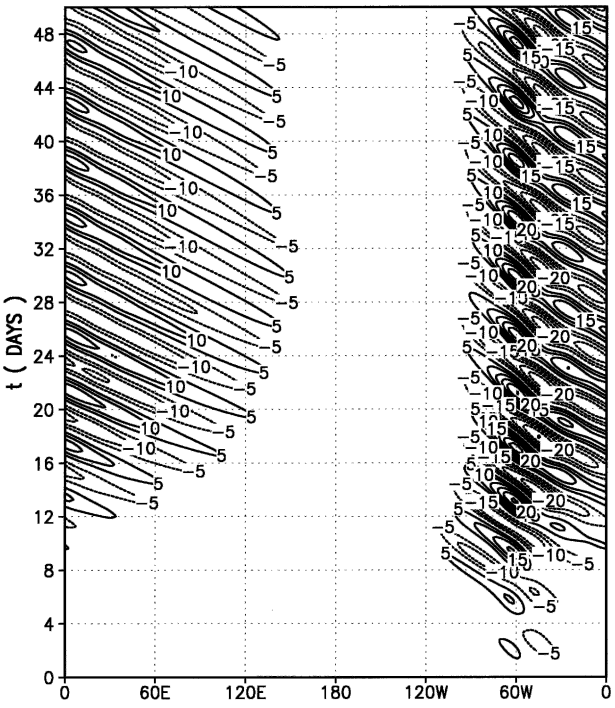

FIG. 5. Time evolution of the meridional component of the wind field along the equator corresponding to the same numerical solution as Figs. 2–4. The v field is shown in m s^{-1}.

easy to note in Fig. 5 that the westward phase propagation and the slow eastward energy dispersion, which are characteristic of the MRGW. The global structure of the MRGW perturbation is also noticeable in Fig. 5.

Figure 6a shows the time evolution of the quadratic part of the total energy of the model, as well as the contribution of each kind of equatorial wave to this integral, for the same numerical solution as Figs. 2–5. Figure 6b is similar to Fig. 6a but corresponds to the linear case. Because of the diagonal representation of $E^{(2)}$ in terms of the expansion coefficients [Eq. (3.3)], the contribution of each type of equatorial wave to the quadratic part of total energy can be easily evaluated. Thus, because of this easy evaluation and the dominance of the component $E^{(2)}$ to the total energy of the model (2.1) ($E^{(2)}$ corresponds to the lowest-order component of the total energy), graphics like those shown in Fig. 6 are useful for analyzing the nonlinear energy exchanges among equatorial waves.

Comparing Figs. 6a and 6b, we can easily conclude that the MRGW are indeed excited by an internal mechanism of energy conversion instead of being directly excited by the thermal source. Figure 6 shows that the excitation of MRGW is much stronger in the nonlinear solution than in the linear one. A careful observation of Fig. 6a also shows that the energy growth of MRGW between $t \approx 7$ and $t \approx 20$ days is reasonably in phase with the energy decrease of RW during the same period. This suggests that the excita-

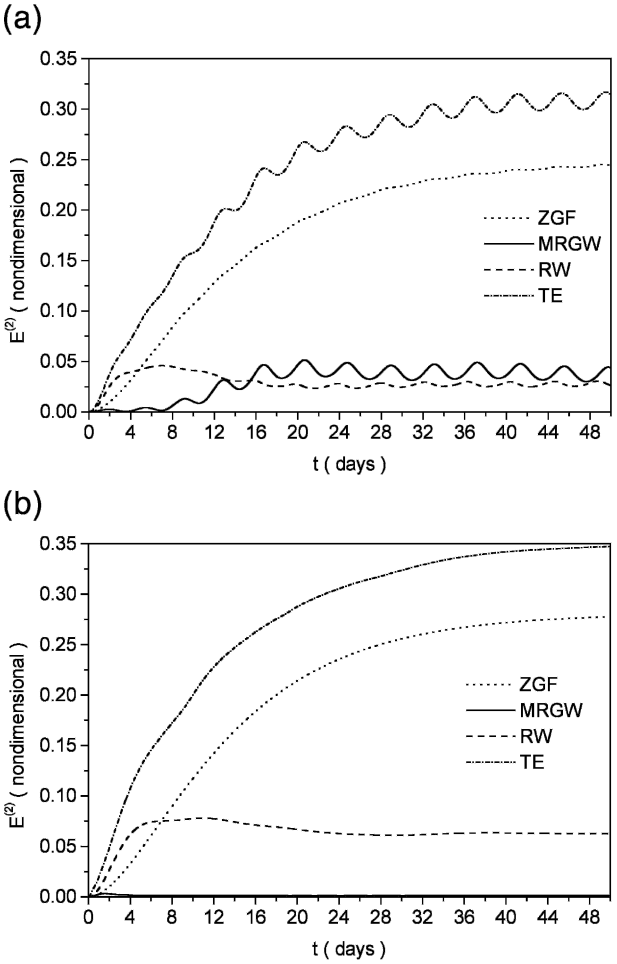

FIG. 6. Time evolution of the TE of the model (2.1), as well as the contribution of ZGF, MRGW, and RW to this integral, for the case of the numerical solution with only quasigeostrophic waves and MRGW inserted in the Rossby category considered in the integration, as (a) nonlinear and (b) linear cases. The energy shown above is nondimensional, using the scales $[L]$ and $[T]$ defined in section 2 with $H = 250$ m.

tion of MRGW may be triggered by an instability of RW excited by the thermal forcing. The decrease of RW energy and the consequent increase of MRGW energy start at $t \approx 7$ days and cease at $t \approx 20$ days, when the numerical solution begins to attain the permanent regime because of the balance between the linear damping and forcing terms, as we can observe by the time evolution of total quadratic energy (TE). In the linear solution (Fig. 6b), the MRGW are very suppressed and the RW-energy decrease starts only at $t \approx$ 12 days and is smoother than in the nonlinear case. The other important feature that can be observed in Fig. 6a is that the modulation of the energy of MRGW in a 4-day cycle, also observed in Fig. 4, is due to a nonlinear energy exchange among RW, MRGW, and zonally symmetric Rossby and Kelvin modes (ZGF), which are absolutely geostrophic. Figure 6a shows that the maxima of quadratic energy associated with MRGW are almost in phase with the minima of RW energy and vice versa. This agreement means that an energy exchange between MRGW and RW occurs. The small off-phase relation between RW energy maxima and MRGW energy minima, as well as the 4-day modulation presented in the time evolution of ZGF energy, imply that the ZGF also participates in the nonlinear interaction between MRGW and RW. This nonlinear energy exchange among RW, MRGW, and the zonally symmetric geostrophic modes is more evident during the permanent regime but also occurs during the transient period. Such persistent nonlinear energy exchange among ZGF, RW, and MRGW is more clearly noticeable in Fig. 7, which is similar to Fig. 6a, but refers to the numerical solution with the exclusion of the zonal mean of the forcing function (4.1). Excluding the zonal average in (4.1), the zonally symmetric geostrophic modes (zonally symmetric Kelvin and Rossby modes) are not directly excited by the source. However, despite the nondirect excitation from the forcing, the zonally symmetric geostrophic modes are excited by the interaction with RW and MRGW, as we can see in Fig. 7 by the growth of ZGF energy during the transient period of the solution. By carefully observing Fig. 7, it seems that, besides the MRGW, the ZGF also receives energy from the RW. Another point that deserves attention is that the magnitude of the MRGW energy in Fig. 7 is slightly lower than in Fig. 6a. This means that the ZGF is also important for the excitation of MRGW.

To test the role of RW for the excitation and time evolution of the energy of MRGW, Fig. 8 shows the time evolution of the quadratic part of total energy and the contribution of each type of equatorial wave to this integral for the same numerical solution as Fig. 6a, but with the RW excluded from the integration. Figure 8 shows that, in the absence of RW, the level of excitation of MRGW is not the same. Furthermore, the MRGW are very suppressed and the total quadratic energy is

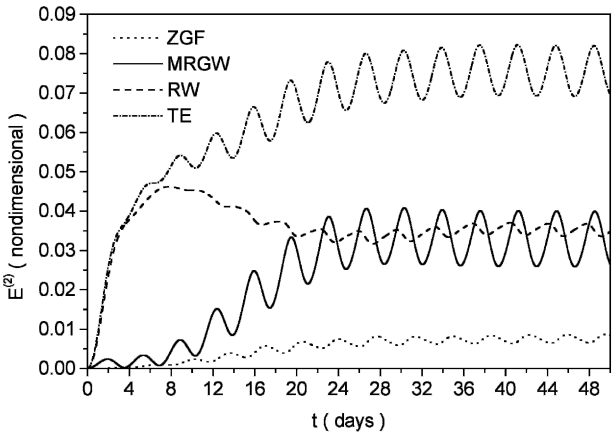

FIG. 7. Similar to Fig. 6a, but with the zonal average of the forcing function (4.1) excluded.

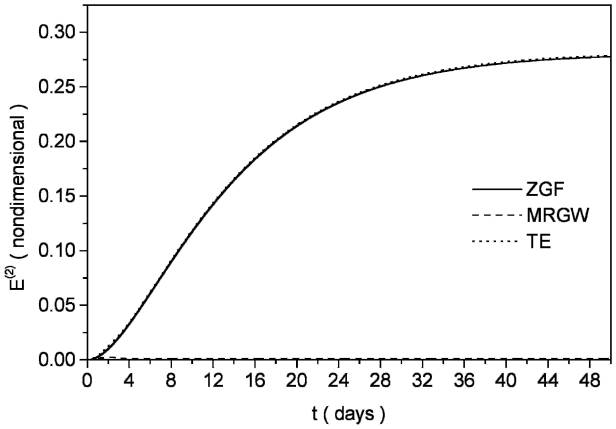

FIG. 8. Similar to Fig. 6a, but with the exclusion of RW.

essentially given by the zonally symmetric geostrophic modes. Unlike the case in which the RW are presented (and the MRGW are excited), the numerical solution in the absence of RW does not show the same vacillation with a 4-day cycle. In this case, like in the linear one, the numerical solution simply tends to attain a stationary regime.

Therefore, the results presented in Figs. 6–8 show that the MRGW excitation observed in Figs. 2–5 is a result of a nonlinear mechanism associated with the internal response of the model to the mass source that roughly represents heat sources associated with typical tropical convective activity. In this sense, the slow modes (ZGF and RW) excited by the thermal forcing generate a basic state that is inherently unstable, supplying energy especially to the MRGW with zonal wavenumbers 4 and 5. According to the comparison between Figs. 7 and 8, the RW are essential to generate the correct basic state in order to feed the MRGW. It is important to explain that the RW with planetary scales (long waves) are more important for exciting the MRGW than the shorter ones (figures not shown). According to the theoretical dispersion relation of the MRGW for $H = 250$ m, the zonal wavenumbers 4 and 5 of these modes have periods of approximately 3.75 and 4.1 days, respectively. Thus, it seems that the 4-day modulation in the time evolution of the modal energetic observed in Figs. 6a and 7 is associated with the phase propagation of the MRGW excited by the quasigeostrophic modes.

In such a scenario, when the maximum perturbation associated with these modes reaches the region near the source, which occurs in a regular 4-day period caused by the phase propagation of these modes, there is a very intense energy exchange among these mixed modes, the RW, and the zonally symmetric geostrophic modes. Figure 9 shows that this energy exchange among these modes induces a vacillation in the nonlinear numerical solution with a cycle determined by the period of the MRGW excited by the quasigeostrophic waves (≈4 days). Figure 9 shows the time evolution of the zonal wind field along the equator corresponding to the same numerical solution as Figs. 2, 3, 4, 5, and 6a.

In fact, Fig. 9 shows that the easterly wind maxima at the equator slowly dispersing westward from the forcing longitude, which are manifestations of planetary

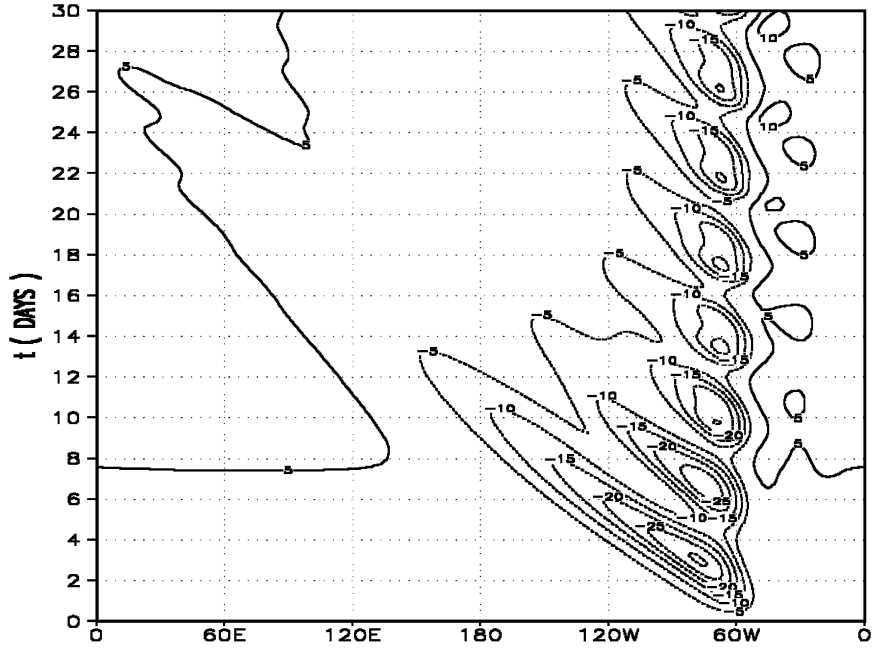

FIG. 9. Time evolution of the zonal wind (m s^{-1}) along the equator corresponding to the same numerical solution as Figs. 2, 3, 4, 5, and 6a.

scale RW, present a clear modulation with a cycle of approximately 4 days. This means that whenever the maxima of perturbations associated with MRGW reach the region near the source, there is a strong energy exchange between the MRGW and the quasigeostrophic waves. Other mechanisms are also known to induce vacillating solutions, such as wave–zonal flow interactions (Pedlosky 1977; Boville 1980) and interference between linear waves with the same wavenumber and different phase speeds (Lindzen et al. 1982). As our results show, nonlinear interactions among waves constituting of a resonant triad can also lead to vacillations.

An intriguing fact about the excitation and time evolution of MRGW energy can be observed in Fig. 10. Figure 10 is similar to Fig. 6a, but refers to the solution with the complete spectrum, that is, with the inertio-gravity waves and the zonally asymmetric Kelvin waves included in the numerical solution. Figure 10 shows that the excitation of MRGW observed in the quasigeostrophic solution does not occur with the inclusion of inertio-gravity waves and $k \neq 0$ Kelvin waves. The well-defined 4-day oscillation in MRGW energy during the first 8 days of integration, as well as the energy decrease of RW after this period, occur exactly as in the quasigeostrophic solutions shown in Figs. 6a and 7. Nonetheless, unlike the quasigeostrophic solution in which the MRGW are excited during the period from $t \approx 7$ to $t \approx 20$ days, the MRGW are very suppressed during this period in the complete nonlinear solution. It is observed from Fig. 10 that the amplitude of the 4-day energy oscillations of the MRGW decreases with the time until the MRGW energy becomes stationary.

The possible explanation for the relatively low signal of MRGW in the complete numerical solution is based on the theory shown in section 3. According to the theoretical analysis carried out in section 3, the nonlinear interactions involving only quasigeostrophic modes practically conserve the quadratic part of total energy and pseudomomentum of the system (2.1). The conservation of $E^{(2)}$ and $P^{(2)}$, in turn, imply a cascade/decascade condition so that the intermediate slowness, weighted by the energy $E^{(2)}$, becomes constant. In this sense, because of the clear separation of the equatorial wave types in the slowness space, when the unstable MRGW with zonal wavenumbers 4 and 5 interact with only quasigeostrophic modes, these mixed modes tend to keep a large part of their energy, resulting in a prominent manifestation of these waves in the solution. On the other hand, in the presence of inertio-gravity and $k \neq 0$ Kelvin waves, the contribution of the $O(c^3)$ terms in the total energy and pseudomomentum is much larger and the constraints given by (3.10) are no longer satisfied. As a consequence, because of the off-resonant interacting triads involving inertio-gravity waves and zonally asymmetric Kelvin waves, the energy transferred from the quasigeostrophic modes to the MRGW tends to be more spectrally redistributed in the complete solution than in the solution that retains only quasigeostrophic modes and MRGW. This spectral redistribution of energy probably implies a small manifestation of the MRGW in the complete solution. As a consequence of this small manifestation of MRGW, the 4-day-cycle vacillation observed in the quasigeostrophic solution does not appear with the inclusion of the fast modes in the integration. Moreover, because of the relation between wavenumber and slowness for the Rossby waves shown in Table 2, the cascade/decascade condition on the slowness space reflects a similar condition on the wavenumber space, as discussed in section 3. Consequently, a direct energy cascade toward the shortest waves, which implies a loss of energy due to the selective biharmonic diffusion, is not permitted in the interactions involving only quasigeostrophic modes. Thus, in the quasigeostrophic solution there is a smaller loss of energy than in the solution that considers the presence of fast modes. This more intense energy loss might also contribute to the small excitation of MRGW in the complete solution. This effect of energy damping induced by the cascade might be mainly caused by the interactions involving resonant harmonics of the fast modes (Ripa 1983b), especially the Kelvin self-interactions. The Kelvin mode self-interactions are more effective than the interactions involving the other kinds of equatorial waves, because, due to the lack of dispersion, all components of the Kelvin mode are always in phase. As a consequence, all of these components of the Kelvin mode are resonantly coupled with each other. The problem of the Kelvin mode self-interactions is studied in detail in Ripa (1982).

Another interesting point on the energy exchange between the MRGW and the quasigeostrophic modes can be observed in Figs. 6a and 7. These figures show that the nonlinear interactions among MRGW, RW, and ZGF imply an oscillation in the TE, even during the permanent regime. This means that there are off-resonant triads in such kinds of interactions. The variation of $E^{(2)}$ due to the nonlinear interactions among

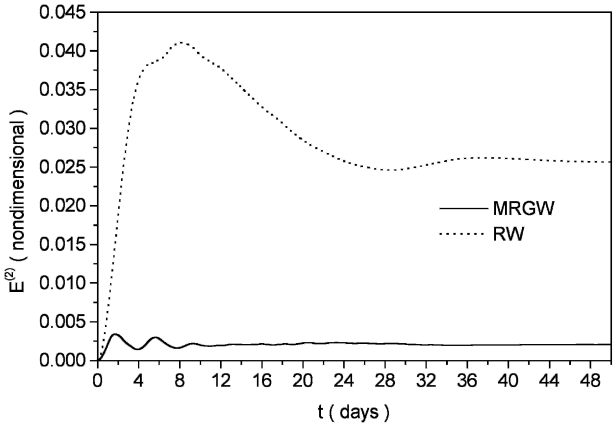

FIG. 10. Similar to Fig. 6a, but referent to the numerical solution with the complete spectrum.

MRGW, RW, and ZGF is also due to a certain gravity wave characteristic present in the $k = 4$ and $k = 5$ MRGW because, according to the theoretical dispersion relation of the equatorial waves (Matsuno 1966), these waves are very close to the limit of separation of the MRGW in terms of Rossby and gravity wave categories. In reality, this reflects the nonexistence of a clear separation of quasigeostrophic and inertio-gravity motions near the equator.

5. Summary and conclusions

Wavelike disturbances with a period of the order of 4 and 5 days and zonal wavenumbers 4 and 5, with a structure very close to the mixed Rossby–gravity waves (MRGW), constitute a prominent characteristic of the tropical atmospheric circulation and have been identified in several observational studies. In the troposphere, such disturbances exercise a strong control on the convective activity over the equatorial region. Both lateral forcing and wave-CISK theories have represented the main efforts to physically explain the excitation of these equatorially trapped perturbations in the troposphere. In this work we performed numerical simulations with a rather simplified model of the tropical atmospheric motions (the shallow water model on the equatorial β plane). Despite not considering either any lateral forcing or parameterization of the feedback between equatorial waves and moist convection, a highly prominent signal of MRGW with a spatial structure of zonal wavenumbers 4 and 5 and a period of the order of 4 days was found in some of our numerical results. Thus, in this paper, a new possible explanation for the relatively high magnitude of the MRGW observed in the tropical atmosphere has been discussed. This explanation is based on the nonlinear interactions among equatorial waves. The nonlinear shallow water equations have been solved using a spectral method that uses the eigensolutions of the linear problem as the expansion basis. A theoretical framework concerning the wave–wave interaction problem in the equatorial waveguide has been developed in section 3 in order to establish a guideline for the physical interpretation of the numerical results shown in section 4.

The numerical results with only quasigeostrophic modes (Rossby and ultralong Kelvin modes) and MRGW inserted in the Rossby category considered in the integration suggest that the MRGW can also be excited by a nonlinear mechanism associated with the internal response of the atmosphere to the heat sources associated with the typical tropical convective activity. In this sense, the slow (quasigeostrophic) modes excited by the thermal forcing generate a basic state that is inherently unstable, supplying energy especially for the MRGW with zonal wavenumbers 4 and 5. The results show that the Rossby waves (especially, the long ones) are essential for generating the correct basic state in order to feed the MRGW. An intriguing point that deserves a further investigation is the instability mechanism that preferentially feeds the MRGW with zonal wavenumbers 4 and 5. Maybe this mechanism of instability is associated with a barotropic instability of the quasigeostrophic basic state generated by the slow mode response to the heat source. The barotropic instability consists of a kinetic energy conversion from the basic state toward the large-scale wavelike eddies and is favored when the momentum flux produced by the eddies is opposite to the gradient of the basic state momentum field. In this sense, it is possible that the spatial structure of the MRGW with zonal wavenumbers 4 and 5 provides the most favorable momentum flux in order to destabilize the quasigeostrophic basic state excited by the heat source.

According to the theoretical dispersion relation of the MRGW for $H = 250$ m, the waves with zonal wavenumbers 4 and 5 have periods of 3.75 and 4.1 days, respectively. Thus, when the maximum perturbation associated with these mixed modes reaches the region near the source, which occurs in a regular 4-day period because of the phase propagation of these modes, there is a very intense energy exchange among these mixed modes, the RW, and the zonally symmetric geostrophic modes. This energy exchange induces a vacillation in the nonlinear numerical solution with a cycle determined by the period of the MRGW ($\approx$ 4 days). The time series of meridional wind and vorticity data at certain points in the Amazon Basin during the period of the ABLE-2b, shown in Santos et al. (2002), present oscillations with periods of the order of 4 to 6 days. Similarly, as shown in Fig. 1, the spectral analysis performed by Santos et al. also detected a rather high signal of 4-to-6-day oscillations in the wind data over the Amazon–Atlantic equatorial sector. Perhaps, the 4-day-cycle vacillation observed in the quasigeostrophic solutions is associated with these local oscillations in the time series of wind data of Santos et al. (2002). The episodes with periods of oscillations in the time series of Santos et al. longer than 4 days, which do not appear in our numerical results, may be close to episodes of intense convective activity in the Amazon, which reduces the phase speed of the MRGW because of the reduction of the effective equivalent height of the system (2.1).

Besides the importance of the quasigeostrophic modes for the excitation of MRGW, the results of this paper also suggest that the predominance of such slow modes in the atmospheric flow is fundamental for maintaining the amplitude of the unstable mixed modes. According to the numerical results shown in section 4, the addition of the fast modes (inertio-gravity and $k \neq 0$ Kelvin waves) tends to inhibit the MRGW excitation. This much-less-intense excitation of MRGW in the complete solution rather than in the solution that retains only quasigeostrophic modes and MRGW can be explained in terms of the framework shown in section 3.

According to this framework, the nonlinear interactions involving only quasigeostrophic modes practically conserve the quadratic part of total energy and pseudomomentum. As a consequence, there is a cascade/decascade condition in these interactions so that the intermediate slowness, weighted by the energy $E^{(2)}$, becomes constant. In this sense, when the unstable MRGW interact with only quasigeostrophic modes, they tend to keep a large part of their energy. On the other hand, in the presence of the fast modes, the contribution of the $O(c^3)$ terms in the total energy and pseudomomentum is much larger and that cascade/decascade condition in the slowness space is no longer satisfied. Then, because of off-resonant interacting triads involving inertio-gravity waves and zonally asymmetric Kelvin waves, the energy transferred from the quasigeostrophic modes to the MRGW tends to be more spectrally redistributed in the complete solution. Moreover, because of the relation between wavenumber and slowness for the Rossby waves shown in Table 2, the cascade/decascade condition on the slowness space reflects a similar condition on the wavenumber space. Consequently, a direct energy cascade toward the shortest waves, which implies a loss of energy due to the selective biharmonic diffusion, is not permitted in the interactions involving only quasigeostrophic modes. Thus, in the quasigeostrophic solution there is a smaller loss of energy than in the solution that considers the fast modes. This more intense energy loss might also contribute to the small excitation of MRGW in the complete solution.

Therefore, the results of this paper suggest that periods of intense activity of MRGW might be close to periods of large predominance of Rossby modes in the equatorial atmospheric flow. On the other hand, periods of intense manifestation of Kelvin wave disturbances may be associated with a weak signal of MRGW. Kelvin and gravity-type disturbances are further intensified when the thermal forcing is transient, that is, the higher the temporal frequency of the heat source, the larger the excitation of Kelvin and inertio-gravity waves (Silva Dias et al. 1983, 1987). For example, periods and places with a high signal of the diurnal cycle on the convective activity might be close to a weak signal of these MRGW observed in tropical atmosphere. An observational investigation about this correlation would be interesting.

Finally, it is important to say that this paper just introduces a new possible guideline to explain the excitation of MRGW-type disturbances observed in the tropical atmosphere. This work does not eliminate the possible role of lateral forcing and interaction with moist convection in exciting these equatorial perturbations. Moreover, the weak signal of MRGW in the complete solution, observed in the numerical results, would also mean that either midlatitude disturbances or interaction with cumulus convection can be important in intensifying the MRGW signal in the tropical atmosphere. Anyway, we have shown here that a further investigation into the nonlinear interacting mechanisms involving the main variability modes that compose the atmospheric motions would explain several features of the atmospheric circulation. Thus, it is important to further explore the interacting mechanisms. The natural next step from the present work is to generalize the ideas presented here by using a more realistic atmospheric model, which considers the presence of more than one single vertical mode. We plan a future study that analyzes the existence of resonant interactions involving the main modes of variability of the large-scale atmospheric circulation (Rossby, inertio-gravity, mixed Rossby–gravity, and Kelvin modes) in a baroclinic atmosphere, that is, associated with different vertical modes. In this future study we will be able to analyze both the nonlinear mechanism of excitation of MRGW studied here and the role of extratropical Rossby waves in exciting equatorially trapped waves. The latter mechanism, which is inherently close to the lateral forcing theory, might be linked to the existence of resonant triads involving synoptic-scale extratropical Rossby waves and equatorially trapped modes, including MRGW.

Acknowledgments. A large part of the work presented in this paper was part of the first author's master thesis developed at University of São Paulo. This thesis was partially financially supported by Fundação de Amparo à Pesquisa do Estado de São Paulo (FAPESP) under GRANT 99/12792-0. During the completion of the thesis, Carlos F. M. Raupp was supported by the program Instituto do Milênio-Avanço Global e Integrado da Matemática Brasileira (IM-AGIMB). The present work is also part of the research proposed by the PROSUR program, financially supported by the IAI. The authors also thank Dr. Jan Paegle and Dr. Julia Paegle for the comments and fruitful suggestions for the present paper.

REFERENCES

Anagnostou, E. N., and C. A. Morales, 2002: Rainfall estimation from TOGA radar observations during LBA field campaign. *J. Geophys. Res.,* **107,** 8068, doi:10.1029/2001JD000377.

Arkin, P. A., and P. J. Webster, 1985: Annual and interannual variability of tropical–extratropical interaction. *Mon. Wea. Rev.,* **113,** 1510–1523.

Bergman, J. W., and M. Salby, 1994: Equatorial wave activity derived from fluctuations in observed convection. *J. Atmos. Sci.,* **51**, 3791–3806.

Boville, B., 1980: Amplitude vacillation on an f-plane. *J. Atmos. Sci.,* **37,** 1413–1423.

Busbridge, I. W., 1948: Some integrals involving Hermite polynomials. *J. London Math. Soc.,* **23,** 135–141.

DeMaria, M., 1985: Linear response of a stratified tropical atmosphere to convective forcing. *J. Atmos. Sci.,* **42**, 1944–1959.

Domaracki, A., and A. Z. Loesch, 1977: Nonlinear interactions among equatorial waves. *J. Atmos. Sci.,* **34,** 486–498.

Dunkerton, T., and M. Baldwin, 1995: Observation of 3–6 day meridional wind oscillations over the tropical Pacific, 1973–

1992: Horizontal structure and propagation. *J. Atmos. Sci.,* **52**, 1585–1601.
Fjörtoft, R., 1953: On the changes in the spectral distribution of kinetic energy for two-dimensional, nondivergent flow. *Tellus,* **5,** 225–230.
Fulton, S. R., and W. H. Schubert, 1985: Vertical normal mode transforms: Theory and application. *Mon. Wea. Rev.,* **113,** 647–658.
Gill, A. E., 1980: Some simple solutions for heat-induced tropical circulation. *Quart. J. Roy. Meteor. Soc.,* **106,** 447–462.
Gruber, A., 1974: The wavenumber-frequency spectra of satellite measured brightness in the Tropics. *J. Atmos. Sci.,* **31,** 1675–1680.
Halverson, J. B., T. Rickenbach, B. Roy, H. Pierce, and E. Williams, 2002: Environmental characteristics of convective systems during TRMM-LBA. *Mon. Wea. Rev.,* **130,** 1493–1509.
Hayashi, Y., 1970: A theory of large-scale equatorial waves generated by condensational heat and accelerating the zonal wind. *J. Meteor. Soc. Japan,* **48,** 140–160.
——, 1974: Spectral analysis of tropical disturbances appearing in a GFDL general circulation model. *J. Atmos. Sci.,* **31,** 180–218.
——, and D. G. Golder, 1978: The generation of equatorial transient planetary waves. *J. Atmos. Sci.,* **35,** 2068–2082.
——, and A. Sumi, 1986: The 30–40 day oscillation simulated in an "aqua planet" model. *J. Meteor. Soc. Japan,* **64,** 4451–4467.
Hayes, W. D., 1974: Introduction to wave propagation in nonlinear waves. *Nonlinear Waves,* S. Leibovich and A. R. Seebass, Eds., Cornell University Press, 331 pp.
Holton, J. R., 1972: Waves in the equatorial stratosphere generated by tropospheric heat sources. *J. Atmos. Sci.,* **29,** 368–375.
Itoh, H., and M. Ghil, 1988: The generation mechanism of mixed Rossby-gravity waves in the equatorial troposphere. *J. Atmos. Sci.,* **45**, 585–604.
Kasahara, A., 1984: The linear response of a stratified global atmosphere to tropical thermal forcing. *J. Atmos. Sci.,* **41,** 2217–2237.
——, and P. L. Silva Dias, 1986: Response of equatorial planetary waves to stationary tropical heating in the global atmosphere with meridional and vertical shear. *J. Atmos. Sci.,* **43**, 1893–1911.
——, and H. L. Tanaka, 1989: Application of vertical normal mode expansion to problems of baroclinic instability. *J. Atmos. Sci.,* **46**, 489–510.
Lamb, V. R., 1973: The response of the tropical atmosphere to middle latitude forcing. Ph.D. thesis, University of California, Los Angeles, 151 pp.
Lau, K.-M., and L. Peng, 1987: Origin of low-frequency (intraseasonal) oscillations in the tropical atmosphere. Part I: Basic theory. *J. Atmos. Sci.,* **44,** 950–972.
Laurent, H., L. A. T. Machado, C. A. Morales, and L. Durieux, 2002: Characteristics of the Amazonian mesoscale convective systems observed from satellite and radar during the WETAMC/LBA experiment. *J. Geophys. Res.,* **107,** 8054, doi:10.1029/2001JD000337.
Lim, H., and C. P. Chang, 1986: Generation of internal and external mode motions from internal heating: Effects of vertical shear and damping. *J. Atmos. Sci.,* **43,** 948–957.
Lindzen, R. S., E. S. Batten, and J.-W. Kim, 1968: Oscillations in atmospheres with tops. *Mon. Wea. Rev.,* **96**, 133–140.
——, B. Farrell, and D. Jacqmin, 1982: Vacillations due to wave interference: Applications to the atmosphere and to annulus experiments. *J. Atmos. Sci.,* **39,** 14–23.
Madden, R. A., and P. Julian, 1972: Description of global-scale circulation cells in the Tropics with a 40–50 day period. *J. Atmos. Sci.,* **29,** 1109–1123.
——, and ——, 1994: Observations of the 40–50 day tropical oscillation—A review. *Mon. Wea. Rev.,* **122,** 814–836.
——, and ——, 1995: Mixed Rossby-gravity waves triggered by lateral forcing. *J. Atmos. Sci.,* **52**, 1473–1486.
Mak, M.-K., 1969: Laterally driven stochastic motions in the Tropics. *J. Atmos. Sci.,* **26,** 41–64.
Maruyama, T., 1967: Large-scale disturbances in the equatorial lower stratosphere. *J. Meteor. Soc. Japan,* **45,** 391–408.
Matsuno, T., 1966: Quasi-geostrophic motions in the equatorial area. *J. Meteor. Soc. Japan,* **44,** 25–43.
Pedlosky, J., 1977: A model of wave amplitude vacillation. *J. Atmos. Sci.,* **34,** 1898–1912.
Pires, P., J. L. Redelsperger, and J. P. Lafore, 1997: Equatorial atmospheric waves and their association to convection. *Mon. Wea. Rev.,* **125**, 1167–1184.
Ripa, P., 1981: On the theory of nonlinear interactions among geophysical waves. *J. Fluid Mech.,* **103,** 87–115.
——, 1982: Nonlinear wave–wave interactions in a one-layer reduced-gravity model on the equatorial β-plane. *J. Phys. Oceanogr.,* **12,** 97–111.
——, 1983a: Weak interactions of equatorial waves in a one-layer model. Part I: General properties. *J. Phys. Oceanogr.,* **13,** 1208–1226.
——, 1983b: Weak interactions of equatorial waves in a one-layer model. Part II: Applications. *J. Phys. Oceanogr.,* **13,** 1227–1240.
Salby, M. L., and R. R. Garcia, 1987: Transient response to localized episodic heating in the Tropics. Part I: Excitation and short-time near field behavior. *J. Atmos. Sci.,* **44**, 458–498.
Santos, I. A., P. L. Silva Dias, and A. R. Torres, 2002: The role of mixed Rossby-gravity waves on the organization of convection in the Amazon. Preprints, *12th Brazilian Congress of Meteorology*, Foz do Iguaçu, Brazil, Brazilian Society of Meteorology, 3995–4001.
Silva Dias, P. L., and J. P. Bonatti, 1985: A preliminary study of the observed modal structure of the summer circulation over tropical South America. *Tellus,* **37A,** 185–195.
——, W. H. Schubert, and M. DeMaria, 1983: Large-scale response of the tropical atmosphere to transient convection. *J. Atmos. Sci.,* **40,** 2689–2707.
——, J. P. Bonatti, and V. E. Kousky, l987: Diurnally forced tropical tropospheric circulation over South America. *Mon. Wea. Rev.*, **115,** 1465–1478.
Takayabu, Y., 1994: Large-scale cloud disturbance associated with equatorial waves. Part I: Spectral features of the cloud disturbances. *J. Meteor. Soc. Japan,* **72**, 433–448.
Tomas, R. A., and P. J. Webster, 1994: Horizontal and vertical structure of cross-equatorial wave propagation. *J. Atmos. Sci.,* **51,** 1417–1430.
Wang, B., and X. Xie, 1996: Low-frequency equatorial waves in vertically sheared zonal flow. Part I: Stable waves. *J. Atmos. Sci.,* **53,** 449–467.
Webster, P. J., and J. R. Holton, 1982: Cross-equatorial response to middle-latitude forcing in a zonally varying basic state. *J. Atmos. Sci.,* **39,** 722–733.
Wheeler, M., and G. N. Kiladis, 1999: Convectively coupled equatorial waves: Analysis of clouds and temperature in the wavenumber-frequency domain. *J. Atmos. Sci.,* **56,** 374–399.
——, ——, and P. J. Webster, 2000: Large-scale dynamical fields associated with convectively coupled equatorial waves. *J. Atmos. Sci.,* **57**, 613–640.
Yanai, M., and T. Maruyama, 1966: Stratospheric wave disturbances propagating over the equatorial Pacific. *J. Meteor. Soc. Japan,* **44,** 291–294.
Zangvil, A., and M. Yanai, 1980: Upper tropospheric waves in the Tropics. Part 1: Dynamical analysis in the wavenumber-frequency domain. *J. Atmos. Sci.,* **37,** 283–298.
——, and ——, 1981: Upper tropospheric waves in the Tropics. Part II: Association with clouds in the wavenumber-frequency domain. *J. Atmos. Sci.,* **38,** 939–953.